IEEE Photonics Journal
An IEEE Photonics Society Publication

Open Access

An On-Orbit Calibration Method of Star Sensor Based on Angular Distance Subtraction

Volume 13, Number 3, June 2021

Liang Wu
Qian Xu
Chao Han
Kaixuan Zhang

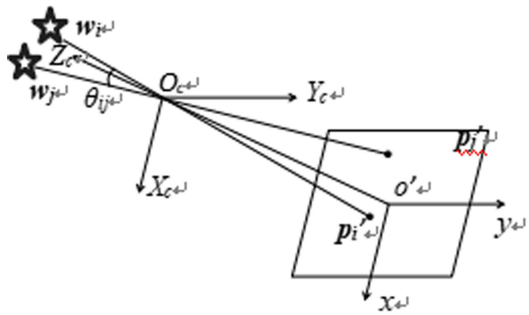

The angular distance matrix of N star points is obtained from the angular distance model

	star 1	star 2	star 3	star 4	star 5	·····	star N
1		a_{12}	a_{13}	a_{14}	a_{15}	·····	a_{1N}
2			a_{23}	a_{24}	a_{25}	·····	a_{2N}
3				a_{34}	a_{35}	·····	a_{3N}
4					a_{45}	·····	a_{4N}
5						·····	a_{5N}
⋮							⋮
N							

Subtract the angular distance

Angular distance subtract method

DOI: 10.1109/JPHOT.2021.3075684

An On-Orbit Calibration Method of Star Sensor Based on Angular Distance Subtraction

Liang Wu, Qian Xu, Chao Han, and Kaixuan Zhang

Department of Computer Science and Engineering, Changchun University of Technology, Changchun 130012, China

DOI:10.1109/JPHOT.2021.3075684

Manuscript received February 7, 2021; revised April 8, 2021; accepted April 21, 2021. Date of publication April 27, 2021; date of current version May 17, 2021. This work was supported in part by the National Natural Science Foundation of China under Grant 61803043, in part by the Education Department of Jilin Province under Grant JJKH20210742KJ, and in part by the Jilin Province Development and Reform Commission under Grant 2021C045-7. Corresponding author: Liang Wu (e-mail: wuliang@ccut.edu.cn).

Abstract: Star sensor needs real-time calibration to improve its navigation accuracy. Compared with other parameters, the position of the principal point is more easily affected by the measurement error, which leads to low calibration accuracy. Conventional star sensors on-orbit calibration methods mainly rely on the angular distance(AD) between stars. The observability of the principal point in this method and the calibration accuracy is not as well as that of other parameters. In this paper, an on-orbit calibration method of star sensor based on the angular distance subtraction(ADS) is proposed. The accuracy of the on-orbit calibration is improved by increasing the observability of the principal point in the calibration process, and the feasibility of this method is verified by the observability analysis. Finally, improved angular distance subtraction(IADS) models are proposed to solve the time-consuming problem of ADS method. In order to demonstrate the performance of the IADS models, simulation calibrations are conducted. The results show that the accuracy of u_0 and v_0 of the IADS method is 62.7% and 15.9% higher than that of AD method when other parameters are set as nominal values. The calibration accuracy of the principal point is improved effectively.

Index Terms: Angular distance subtraction, calibration, on-orbit, principal point, star sensor.

1. Introduction

Star sensor is a kind of navigation system and it is also the optical attitude sensor with the highest precision at present [1], [2], thus it has become one of the indispensable navigation equipment on the spacecraft [3], [4]. The calibration error of optical parameters will affect the measurement accuracy of star sensor seriously. Among these optical parameters, the principal point is the only parameter that describes the optical axis, which has a significant impact on the measurement results. Therefore, in order to improve the accuracy of star sensor, it is necessary to calibrate the principal point of star sensor.

The principal point calibration methods of star sensor are divided into ground-based calibration and on-orbit calibration. The ground-based calibration of star sensor is carried out under the normal temperature and pressure, which is quite different from the on-orbit application environment. The intrinsic parameters of star sensor deviate due to the vibration during launch and the change of

instrument working environment [5], [6]. Therefore, it is necessary to calibrate the star sensor parameters on-orbit to improve the working accuracy and autonomous ability.

M. D. Shuster [7] proposed an on-orbit error estimation method based on the relative alignment installation error of attitude sensors. After that, many on-orbit calibration methods of star sensors and other attitude sensors have been carried out. At present, most of the calibration methods are based on angular distance. M. Samaan [8] proposed an optimization estimation method, which can minimize the calculation error of angular distance in the image and the corresponding catalog. H.B. Liu [9] used the sine value of angular distance to establish the observation equation to calibrate the parameters. Z. Wang [10] established the angular distance error model and determined the variation range of the observation angular distance error. J. Enright [11], [12] suggested using the angular distance directly and adopting a new camera model for calibration. Although the method of angular distance is widely used, the calibration accuracy of the principal point is much worse than that of other parameters [13], [14]. H. J. Zhong [15] put forward a method which calibrated the principal point first, then the focal length, and finally calibrated the distortion parameters. However, the calibration method of the principal point needs manual intervention and the data processing is complex. J. H. Yang [16] proposed a high-precision camera principal point calibration method. In this method, the laser beam emitted by the laser is parallel to the camera optical axis, so that the spot is projected onto the screen, and the screen is moved several times to obtain the spot images of different positions. Due to the complexity of the process, it is not suitable for star sensor calibration which needs real-time data. P. W. Nie [17] improved the calibration accuracy by weighting the principal point and focal length, and eliminating the star points with large random measurement noise. Whereas this method did not fundamentally discuss the calibration accuracy of the principal point. It can be seen that there is little research on the accuracy of the principal point in the calibration process, especially in the on-orbit calibration application of the star sensor, which needs to be further discussed.

The remainder of this paper is organized as follows. The camera model is introduced in Section 2. In Section 3, an optical parameter calibration method based on angular distance subtraction(ADS) is introduced. The feasibility of this method is verified by observability analysis, and an optimal improved angular distance subtraction(IADS) model is discussed. In Section 4, experiments are carried out to verify and evaluate the performance of the AD method, ADS method, and IADS method. Finally, some conclusions are drawn.

2. Camera Model

The camera model is a mathematical description of the physical imaging process from the scene object to the image plane, which can be regarded as a pinhole model. The calibration of star sensor generally includes intrinsic parameters and extrinsic parameters [18]. In this paper, we mainly discuss the intrinsic parameters, especially the calibration of the principal point in the intrinsic parameters, and involving three coordinate frames, as shown in Fig. 1. Fig. 1(a) shows the relationship between the camera frame and the physical image frame, and Fig. 1(b) shows the relationship between the physical image frame and the image frame.

1) Camera frame($O_c - X_cY_cZ_c$): Taking the optical center of the camera as the origin of coordinates, the X_c-axis and Y_c-axis are parallel to the horizontal and vertical axes of the image frame respectively, and the optical axis of the camera is the Z_c-axis.
2) Physical image frame($o' - xy$): Taking the intersection point of CCD image plane and camera optical axis as the coordinate origin o', x-axis and y-axis are parallel to the two vertical edges of image plane respectively. The image frame represents the position of pixels in the image with physical units (such as millimeters).
3) Image frame($o - uv$): Taking the top left corner of the CCD image plane as the origin, the u-axis and v-axis are parallel to the x-axis and y-axis of the physical image frame respectively. Image frame is a coordinate system based on pixel.

Let $w = [X, Y, Z]^T$ be an arbitrary star unit vector in the camera frame, and its ideal projection under the image frame is $p = [u, v]^T$. The perspective projection relationship between w and p can

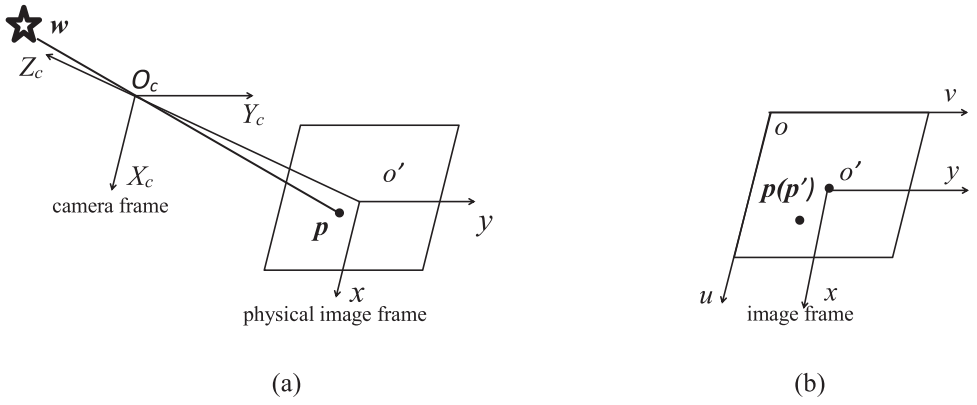

Fig. 1. Reference frames. (a) Camera frame and physical image frame; and (b) physical image frame and image frame.

be expressed as

$$\begin{bmatrix} u \\ v \\ 1 \end{bmatrix} = \frac{1}{Z} \begin{bmatrix} f_u & 0 & u_0 \\ 0 & f_v & v_0 \\ 0 & 0 & 1 \end{bmatrix} \begin{bmatrix} X \\ Y \\ Z \end{bmatrix} \tag{1}$$

where $[u, v, 1]^T$ is the homogeneous coordinate of the point p, f_u and f_v are the focal lengths of pixels in the u-axis and v-axis directions, respectively. (u_0, v_0) is the coordinate of the principal point.

In fact, all lenses have distortion. Considering the distortion, the following formulas can be used to describe the nonlinear model of the camera:

$$\begin{cases} u_d = u + \delta_u(u, v) \\ v_d = v + \delta_v(u, v) \end{cases} \tag{2}$$

where (u,v) is the distortion-free coordinate, (u_d, v_d) is the coordinate under the nonlinear model, that is, the image coordinate considering the geometric distortion of lens. $\delta_u(u, v)$ and $\delta_v(u, v)$ are distortions in u and v direction, respectively. The distortion of camera can be divided into three types: radial distortion, eccentric distortion and thin prism distortion. Since radial distortion has the greatest impact, and higher-order distortion may lead to numerical instability [19], we only consider the first-order and second-order radial distortion here:

$$\begin{cases} \delta_u(u, v) = u(k_1 r^2 + k_2 r^4) \\ \delta_v(u, v) = v(k_1 r^2 + k_2 r^4) \end{cases} \tag{3}$$

where k_1 and k_2 are radial distortion coefficients. r^2 is

$$r^2 = \frac{(u - u_0)^2}{f_u^2} + \frac{(v - v_0)^2}{f_v^2} \tag{4}$$

3. Calibration Model of Star Sensor

3.1 Angular Distance Subtraction Method can Enlarge the Calculation of the Principal Point

At present, most star sensor calibration uses angular distance. The angular distance model of star sensor is shown in Fig. 2. θ_{ij} is angular distance between the stars *i* and *j*.

The focal length of the star sensor is *f*, *w* and *v* are the direction vectors of the star in the star sensor frame and the celestial frame, respectively. The coordinate of the projection point of star *i*

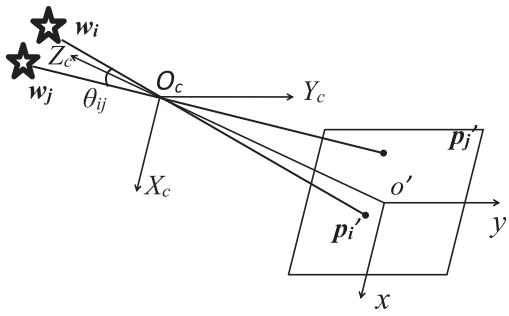

Fig. 2. The angular distance model of star sensor.

in the physical image frame of star sensor imaging is (x_i, y_i), then,

$$w_i = \frac{1}{\sqrt{(x_i - x_0)^2 + (y_i - y_0)^2 + f^2}} \begin{bmatrix} -(x_i - x_0) \\ -(y_i - y_0) \\ f \end{bmatrix} \tag{5}$$

$$v_i = \begin{bmatrix} \cos\alpha_i \cos\delta_i \\ \sin\alpha_i \cos\delta_i \\ \sin\delta_i \end{bmatrix} \tag{6}$$

where (x_0, y_0) represents the principal point to be calibrated, α_i and δ_i represent the right ascension and declination of the star i respectively.

According to the invariance principle of orthogonal transformation of angular distance, without considering distortion and noise, the angle between the orientation vectors w_i, w_j of stars i, j in the star sensor frame is equal to the angle of the corresponding position vectors v_i, v_j in the celestial frame [8], which can be expressed as

$$\cos\theta_{ij} = {w_i}^T w_j = {v_i}^T v_j \tag{7}$$

Substituting (5) into (7) yields:

$$\mathrm{v_i}^T v_j = \frac{N_{ij}}{D_i D_j} = g_{ij}(x_0, y_0, f) \tag{8}$$

where

$$\begin{cases} N = (x_i - x_0)(x_j - x_0) + (y_i - y_0)(y_j - y_0) + f^2 \\ D_i = \sqrt{(x_i - x_0)^2 + (y_i - y_0)^2 + f^2} \\ D_j = \sqrt{(x_j - x_0)^2 + (y_j - y_0)^2 + f^2} \end{cases} \tag{9}$$

The angular distance (AD) method is based on (7), (8), and (9) for calibration. The disadvantage of these formulas is that the focal length is much larger than the size of the CCD, which leads to the poor observability of the principal point. In order to solve this problem, we adopt a two-step method to calibrate the parameters. In the first step, the AD method is used to calibrate all the parameters. In the second step, the focal length and distortion obtained in the first step are taken as fixed values, and the principal point are calculated by angular distance subtraction(ADS) method. The ADS method is as follows:

Suppose that there are three stars i, j, and k, we can calculate $v_i^T v_j$ and $v_j^T v_k$ by using (8), and then the two formulas are subtracted and expressed by S.

$$S = v_i^T v_j - v_j^T v_k = \frac{N_{ij}}{D_i D_j} - \frac{N_{jk}}{D_j D_k} \tag{10}$$

If the FOV of the star sensor is small, then the focal length is much larger than the size of CCD, then

$$D_i D_j \approx D_j D_k \tag{11}$$

Equation (11) can be approximated to $D_a D_b$, a, b as arbitrary two stars, $a \neq b$. Equation (10) can be written as

$$S = \frac{N_{ij} - N_{jk}}{D_a D_b} = \frac{x_i x_j - x_i x_0 + y_i y_j - y_i y_0 - x_j x_k + x_0 x_k - y_j y_k + y_0 y_k}{D_a D_b} = g_{ijk}(x_0, y_0) \tag{12}$$

The focal length has been eliminated in (12), and enlarging the calculation of the principal point, then the observability of the principal point and the calibration accuracy are improved.

Finally, according to the general calibration process [12], the Extended Kalman Filter (EKF) [20] is used to iterate the star points image sequence, and the calibrated parameters can be obtained.

The state transition model is:

$$x_k = I_{2\times 2} \cdot x_{k-1} \tag{13}$$

where x_k is the principal point to be calibrated. $k-1$ and k represent the $k-1_{\text{th}}$ and k_{th} images, respectively. $I_{2\times 2}$ is an identity matrix.

The measurement model is:

$$z_k = h(x_k) + n_c \tag{14}$$

where z_k is the matrix formed by the angular distance subtraction, which is calculated from the position vector in celestial frame. $h(x_k)$ is the process of using the star sensor calibration model and image points to calculate the angular distance subtraction matrix. n_c is the measurement error caused by noise.

The EKF prediction equations are:

$$x_k^- = x_{k-1}^- \tag{15}$$

$$P_k^- = P_{k-1}^- + Q, \tag{16}$$

where P_k^- is the prior estimated covariance at time k, and Q is the covariance matrix of the system process.

The EKF update equations are:

$$K_k = P_k^- H_k^T (H_k P_k H_k^T + R)^{-1}, \tag{17}$$

$$x_k = x_k^- + K_k(z_k - h(x_k^-)), \tag{18}$$

$$P_k = (I - K_k H_k) P_k^-, \tag{19}$$

where R is the covariance matrix of the measurement noise. H_k is a Jacobian matrix.

3.2 The Situations That Cannot Be Ignored in the Above Algorithms

In actually, special situations may appear due to the uncertainty of the location of the stars. For example, the focal length is 16mm, and the field of view is a 4° circle. Star j and star k are close to the boundaries of the image plane while star i is close to its center, as shown in Fig. 3.

Then we can get the $D_i D_j$ is about 256.1520, and the $D_j D_k$ is about 256.3122, the difference between $D_i D_j$ and $D_j D_k$ could be small but significant. In this case, using (11) to equate them will bring some error. Therefore, in the actual experiment, we did not equalize $D_i D_j$ and $D_j D_k$, but directly used the result of subtraction of (10), so that these points at special locations would not cause errors. Equations (11) and (12) only explain why the subtraction of angular distance between stars can magnify the calculation of the principal point. Even without (11), the influence of focal length can also be reduced.

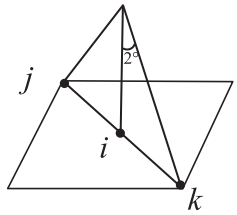

Fig. 3. A special situation of stars position.

3.3 Observability Analysis

Observability can reflect the ability of state estimability, and is an index to evaluate the feasibility of the system. In other words, under different models, the same input deviation may lead to different output deviation. If the magnitude of the output deviation is large, that is, the input deviation is smaller under the same output deviation, the observability is better and the system is more feasible, and vice versa [21].

According to the definition of observability, we can obtain

$$\delta z_k = H_k \delta x \tag{20}$$

where δx is input deviation, δz_k is output deviation, H_k is Jacobian matrix. The observability of Jacobian matrix is analyzed by using singular value decomposition of observable matrix, (20) can be expressed as

$$\delta z_k = P_k \sum_k Q_k \delta x \tag{21}$$

where P_k and Q_k are orthogonal matrices of left singular vector and right singular vector, respectively. $\sum_k$ is a $2 \times N$ diagonal matrix, and the diagonal elements are nonzero singular value σ_i ($i =$ 1-2).

Since P_k and Q_k are orthogonal matrices, we can calculate that

$$\|\delta z_k\|_2^2 = \sum_{i=1}^{2} \sigma_i^2 \|\delta x\|_2^2 \tag{22}$$

where $\|\delta x\|_2$ and $\|\delta z_k\|_2$ are the two-norms of δx and δz_k, respectively.

The infimum of the output deviation is:

$$\|\delta z_k\|_2^2 \geq 2\sigma_{\min}^2 \|\delta x\|_2^2 \tag{23}$$

where $\sigma_{\min}$ is the minimum singular value(MSV) of the observability matrix. The larger the $\sigma_{\min}$, the larger the minimum output deviation and the better observability.

According to the above analysis, we performed singular value decomposition for Jacobian matrix H_k in (16), and calculated the MSV $\sigma_{\min}$ for each frame, then compared the observability of AD method with ADS method. As shown in Fig. 3, it is obvious that the MSV of the ADS method is much higher than that of the AD method, which indicates that the ADS method has better observability.

However, using too many angular distance subtraction combinations will increase the amount of calculation inevitably. As a result, the efficiency of the star sensor is low and can not meet the real-time requirements. Therefore, on the premise of not reducing the calibration accuracy, we improve ADS method to reduce the amount of star angular distance subtraction combinations and increase the calibration efficiency.

3.4 Improved Angular Distance Subtraction Models

In order to improve the efficiency of the ADS method, we proposed four improved models.

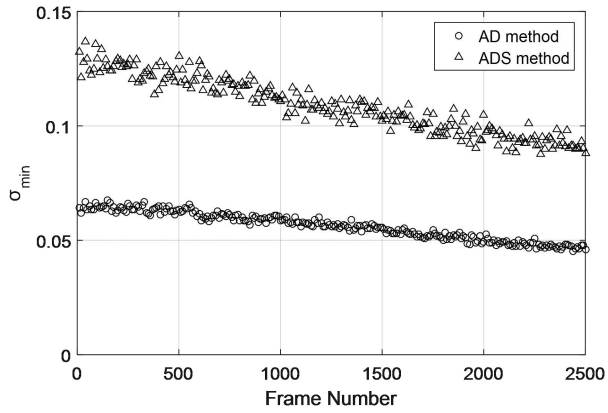

Fig. 4. The observability analysis of AD method and ADS method.

TABLE 1
Uniformity of Stars

	IADS1		IADS2		IADS3		IADS4	
	Using times	Usage rate	Using times	Usage rate	Using times	Usage rate	Using times	Usage rate
star 1	11	13.75%	14	11.67%	15	10.71%	19	10.56%
star 2	11	13.75%	18	15%	21	15%	28	15.56%
star 3	12	15%	18	15%	22	15.71%	28	15.56%
star 4	12	15%	19	15.83%	23	16.43%	29	16.11%
star 5	12	15%	18	15%	22	15.71%	28	15.56%
star 6	11	13.75%	18	15%	21	15%	28	15.56%
star 7	11	13.75%	15	12.5%	16	11.47%	20	11.11%

Suppose that there are N stars in a star map. According to (7), the angular distance of any two stars can be calculated, and the angular distance matrix as shown in the Fig. 4 can be obtained. Since the matrix is symmetric, we only take the upper part of the triangular matrix, and give the following four improved subtraction models.

Model 1: Each row is subtracted horizontally, for example, $a_{12} - a_{13}$, $a_{13} - a_{14}$, $a_{14} - a_{15}$. Then the last one in each row is subtracted from the first in the next row, for example, $a_{1N} - a_{23}$, $a_{2N} - a_{34}$ … …

Model 2: In the same way as Model 1, each row is subtracted horizontally, for example, $a_{12} - a_{13}$, $a_{13} - a_{14}$, $a_{14} - a_{15}$ … …And then subtract each column in turn, for example, $a_{13} - a_{23}$, $a_{14} - a_{24}$, $a_{24} - a_{34}$ … …

Model 3: On the basis of Model 2, add diagonal subtraction, for example, $a_{12} - a_{23}$, $a_{23} - a_{34}$, $a_{34} - a_{45}$ … …

Model 4: On the basis of Model 3, in addition to diagonal subtraction, add all diagonal subtractions, for example, $a_{13} - a_{24}$, $a_{14} - a_{25}$, $a_{15} - a_{26}$ … …

We analyzed the uniformity of the above four improved models. Taking 7 stars as an example, the using times and usage rate of each star are shown in Table 1. As can be seen from Table 1, the improved angular distance subtraction 1(IADS1) model has the most uniform usage rate of each star, but the stars used less times, which may affect the calibration accuracy. Improvement angular distance subtraction 3(IADS3) and improvement angular distance subtraction 4(IADS4) are used more times of each star, but the usage rate is not uniform compared with IADS1 and IADS2. Therefore, improvement angular distance subtraction 2(IADS2) is better in terms of using times and usage rate.

4. Experiments and Discussion

We simulated the star data, with a 19.14° × 11.18° FOV, for a 1920 × 1080 pixel-array star sensor at a 2-Hz update rate. The simulation data consisted of three datasets: a set of 3D star vectors in

TABLE 2
Parameters and Nominal Values

Parameters	u_0 (pixel)	v_0 (pixel)	f(mm)	k_1	k_2
Nominal Values	970	550	16	-0.5	0.5

TABLE 3
Comparison of AD Method and ADS Method

the range of star number	Method	Δu_0(pixel)	Δv_0(pixel)	$\Delta Pitch$(")	ΔYaw(")	$\Delta Roll$(")	T(ms)
6~8	AD	0.82	0.44	0.61	0.53	0.10	0.84
	ADS	0.39	0.47	0.37	0.25	0.10	2.14
13~15	AD	0.89	0.28	0.60	0.58	0.02	2.45
	ADS	-0.19	-0.13	0.15	0.13	0.02	23.12
17~21	AD	-0.45	-0.32	0.36	0.30	0.05	6.31
	ADS	-0.10	-0.22	0.13	0.07	0.05	501.44

the inertial frame, a set of corresponding 2D star coordinates in the image frame, and the set of 2D star coordinates with normally-distributed noise. In order to avoid the influence of other parameters on the accuracy of the principal point, we set the focal length and distortion parameters as nominal values, and only calibrate the principal point. The parameters and nominal values are shown in Table 2.

4.1 Test 1: Comparison of Angular Distance Method and Angular Distance Subtraction Method

By setting the limit visual magnitude of the star sensor, we obtained data with different number of stars for experiments. The intrinsic parameters and distortion parameters of AD method also use the nominal values in Table 2, and we calibrate the principal points only. The number of stars per frame in the three experiments ranged from 6 to 8, 13 to 15, and 17 to 21, respectively, with the limiting visual magnitudes of 4.6, 5, and 5.5, respectively. Normal distribution noise with mean value of 0, standard deviation of 0.5 pixel is added to 2D star coordinates, and the results are shown in Table 3.

In Table 3, Δu_0 and Δv_0 represent the difference between the calibrated principal point results and the nominal values in Table 2. Pitch, yaw and roll are the x-axis, y-axis and z-axis of Euler angle vector respectively. $\Delta Pitch$, ΔYaw and $\Delta Roll$ are the difference between the Euler angle calculated by using the simulation data with noise and the calibration results of the principle point, and which calculated by the set standard parameters. T is the average elapsed time for each frame. Fig. 6 is a radar plot of Table 3. According to the results, the principal point calibration accuracy of the ADS method is better than that of the AD method obviously. As expected, the ADS method is time-consuming, especially when the number of stars is large. It will seriously affect the calibration efficiency of star sensor and fail to meet the real-time requirements. We experimented with four improvement models.

4.2 Comparison of Four Improved Models

In order to verify the analysis of the using times and usage rate of the improved models in Section 3.4, the following experiments were carried out. Using the data of 7.7 stars per frame. Add normal distribution noise with mean value of 0 and standard deviation of 0.5 pixels. The results are shown in Table 4.

It can be seen from Table 4 that although the star points of IADS1 are used more evenly, the number of star angular distance subtraction combinations is relatively small, which leads to poor calibration effect to a certain extent. The uniformity of star points used in IADS3 and IADS4 is poor,

	star 1	star 2	star 3	star 4	star 5	·····	star N
1		a_{12}	a_{13}	a_{14}	a_{15}	·····	a_{1N}
2			a_{23}	a_{24}	a_{25}	·····	a_{2N}
3				a_{34}	a_{35}	·····	a_{3N}
4					a_{45}	·····	a_{4N}
5						·····	a_{5N}
⋮							⋮
N							

Fig. 5. Angular distance matrix.

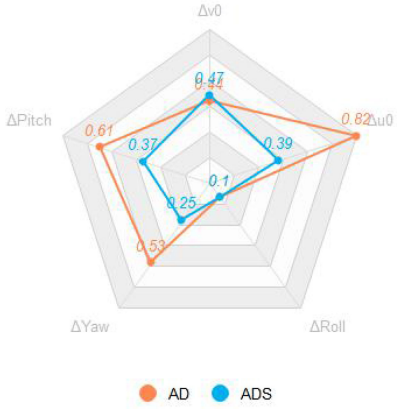

Fig. 6. Comparison of AD method and ADS method.

TABLE 4
Comparison of Four Improved Models

	Δu_0(pixel)	Δv_0(pixel)	$\Delta Pitch$(″)	ΔYaw(″)	$\Delta Roll$(″)	T(ms)
ADS	0.39	0.47	0.37	0.25	0.10	2.14
IADS1	0.24	1.33	0.52	0.15	0.11	1.46
IADS2	-0.17	0.46	0.04	0.11	0.10	1.87
IADS3	0.35	0.90	0.06	0.23	0.10	2.02
IADS4	0.13	0.72	0.29	0.08	0.10	2.04

which will lead to unstable calibration results. Moreover, IADS4 uses a large number of angular distance subtraction combinations. Although the calibration effect is better than that of IADS1, the time consumption is increased significantly. In contrast, although the u_0 accuracy of IADS2 is 23.2% lower than that of IADS4, the accuracy of v_0 is improved by 35.4%, and the usage rate of star points is more uniform than that of IADS4. It can also be seen from Euler angle that the ΔYaw of IADS2 is similar to that of IADS4, but $\Delta Pitch$ is reduced significantly. Compared with ADS method, all indexs of IADS2 are better than ADS method, and the time consumption is reduced by 12.6% compared with ADS method per frame. Therefore, the calibration effect of IADS2 is better, which is consistent with our analysis in Section 3.4. Fig. 7 is a radar plot comparing the four models, from which we can clearly see the advantages of IADS2.

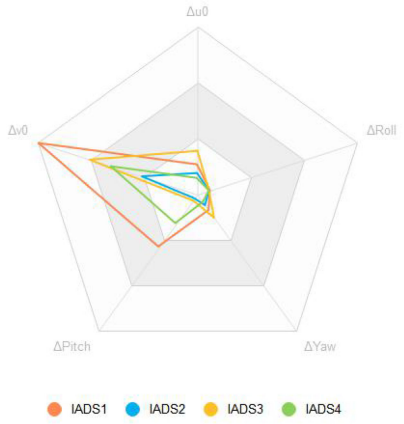

Fig. 7. Comparison of Four Improved Models.

TABLE 5
Comparison of AD Method, SVD Method and IADS2 Method

Noise	Method	Δu_0(pixel)	Δv_0(pixel)	$\Delta Pitch$(")	ΔYaw(")	$\Delta Roll$(")	T(ms)
	AD	0.27	0.35	0.26	-0.18	0.04	0.86
0.2	SVD	0.13	0.37	0.18	-0.09	0.04	0.76
	IADS2	0.10	0.29	0.15	-0.07	0.04	1.37
	AD	0.82	0.44	0.61	-0.53	-0.10	0.86
0.5	SVD	0.60	1.24	0.71	-0.39	-0.11	0.78
	IADS2	-0.17	0.46	0.04	0.11	-0.10	1.31
	AD	1.37	0.87	1.06	-0.90	-0.17	0.84
0.8	SVD	0.99	2.00	1.16	-0.65	-0.18	0.74
	IADS2	-0.30	0.70	0.03	0.20	-0.15	1.36

4.3 Test 3: Comparison of Improved Angular Distance Subtraction 2 Method With Angular Distance Method and Singular Value Decomposition Method

On the basis of Test 2, we compare the IADS2 method with the AD method and the previously proposed singular value decomposition(SVD) method [22]. The average number of stars per frame was 7.7 stars, and three sets of experiments were conducted. The standard deviations of experimental noise in each group were 0.2, 0.5, and 0.8 pixels, respectively. The experimental results are shown in Table 5.

As can be seen from Table 5, when the noise standard deviation is 0.2 pixels, the Δu_0 and Δv_0 accuracy of the IADS2 reduced by about 62.7%, 15.9% compared with the AD method, respectively, and reduced by about 22.3%, 20.4% compared with the SVD method, respectively. In terms of Euler angle, $\Delta Pitch$ and ΔYaw also decreased significantly. When the noise standard deviation is 0.5 pixel, the Δv_0 of the IADS2 method is 5.2% worse than that of AD method, but Δu_0 is better than AD method and SVD method by 79.3% and 71.6%, respectively. When the standard deviation of noise is 0.8 pixels, all indexes of IADS2 method are better than AD method and SVD method. Fig. 5 shows the variation of Euler angles of the three methods when the noise standard deviation is 0.5 pixel. As can be seen from Fig. 5, with the convergence of parameters, the $\Delta Pitch$ and ΔYaw of IADS2 method are smaller than those of AD method and SVD method significantly. Because the deviation of the principal point only involves the movement in the plane, no rotation, so this experiment can only affect pitch and yaw, but not roll. The main factor affecting the roll is the uncertainty of star points position [23], and the three methods use the same set of star points data, so the difference between the results of $\Delta Roll$ is very small.

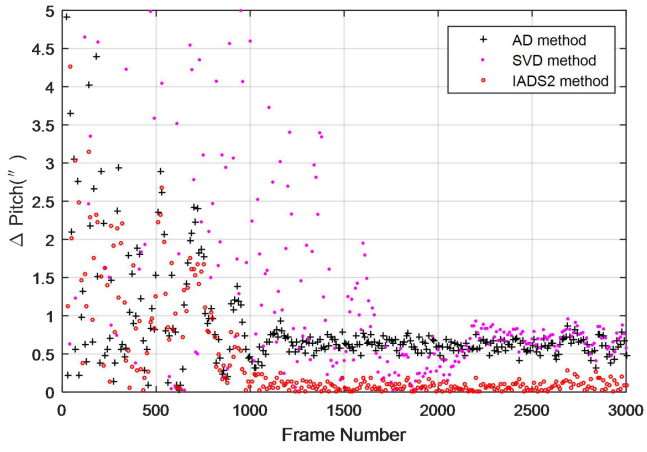

(a)

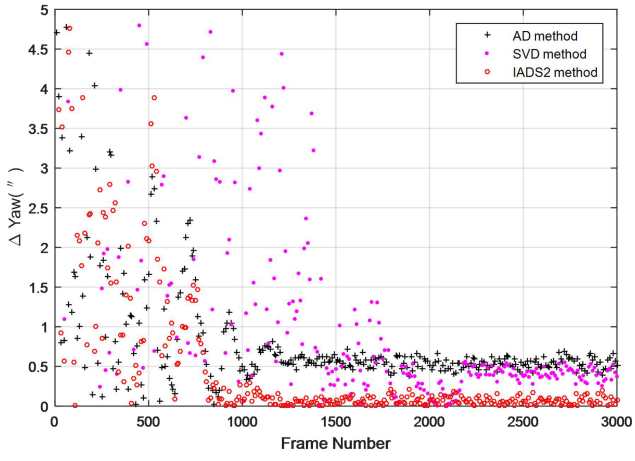

(b)

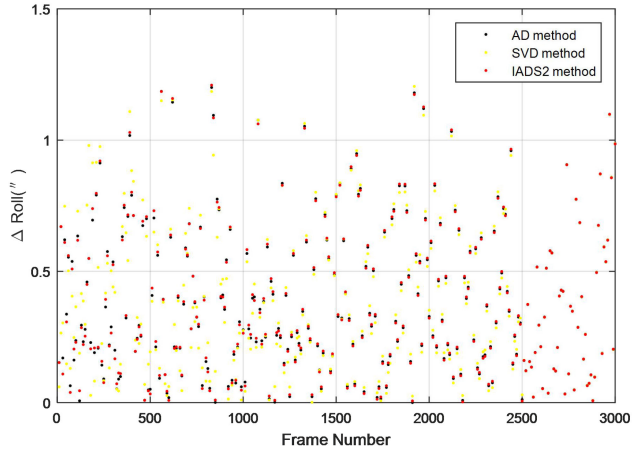

(c)

Fig. 8. Euler Angles of AD method, SVD method, and IADS2 method. (a) $\Delta Pitch$; (b) ΔYaw; and (c) $\Delta Roll$.

TABLE 6
Calibration for all Parameters

	Δu_0 (pixel)	Δv_0 (pixel)	$\Delta Pitch('')$	$\Delta Yaw('')$	$\Delta Roll('')$	f(mm)	k_1	k_2	T(ms)
AD	1.02	-0.81	0.37	-0.67	0.01	-0.00014	0.0011	-0.0074	2.1
SVD	0.93	0.15	0.60	-0.62	0.02	-0.00011	-0.0013	0.1716	1.4
IADS2	0.70	0.21	0.46	-0.45	-0.01	-0.00048	0.0060	-0.2279	2.0

4.4 Test 4: Comparison all Parameters of Angular Distance Method, Singular Value Decomposition Method and Improved Angular Distance Subtraction 2 Method

In order to fully analyze the performance of IADS2 method, we carried out calibration experiments for all parameters. The experimental conditions are the same as Test 2. The calibration results are shown in Table 6.

We found that the focal length and distortion parameters calibration of IADS2 method is not as good as AD method and SVD method, but the calibration accuracy of the principal point is still improved. Therefore, AD method or SVD method can be used to calibrate other parameters before calibrating the principal point to achieve high-precision calibration.

5. Conclusion

In this paper, an on-orbit calibration method of star sensor based on angular distance subtraction is presented. Firstly, the camera model is introduced. Then, on the basis of the invariable principle of orthogonal transformation of angular distance between the stars, the star angular distances were subtracted to enlarge the calculation of principal point. The feasibility of this method is proved by observability analysis. Since too many star angular distance subtraction combinations will lead to long calibration time, we proposed four improved models and discussed the best improved model IADS2 to improve the calibration efficiency. The simulation results are consistent with our analysis. Compared with the AD method, the IADS2 method has higher calibration precision of the principal point, and the time consuming is not different from the AD method. Therefore, it is more suitable for the real time calibration of star sensor. Although the performance of ADS method is good, more tests should be carried out under different conditions due to the first proposal. In addition, further research is needed on the star angular distance subtraction combination model.

Acknowledgment

First of all, we would like to thank the reviewers for their valuable suggestions. The author Liang Wu is also supported by the China Scholarship Council. Both of them are gratefully acknowledged.

References

[1] B. Pang, K. Li, and L. Tang, “Error analysis and compensation for star sensor,” *Aerosp. Control Application*, vol. 43, no. 1, pp. 17–24, Feb. 2017.
[2] X. P. Li, P. C. Ren, and Y. Gao, “Distributed FOV fusion algorithm for multiple heads star tracker,” *Flight Control and Detection*, vol. 1, no. 1, pp. 71–76, Jul. 2018.
[3] X. L. Wang, X. J. Guan, and J. C. Fang, “A high accuracy multiplex two-position alignment method based on SINS with the aid of star sensor,” *Aerosp. Sci. Technol.*, vol. 42, pp. 66–73, Apr. 2015.
[4] B. Liang, H. L. Zhu, and T. Zhang, “Research status and development tendency of star tracker technique,” *Chin. Opt.*, vol. 9, pp. 16–29, Feb. 2016.
[5] X. G. Wei, G. J. Zhang, and Q. Y. Fan, “ Star sensor calibration based on integrated modelling with intrinsic and extrinsic parameters,” *Measurement*, vol. 55, pp. 117–125, Sep. 2014.
[6] H. Jin, X. N. Mao, and X. P. Li, “Research on star tracker On-orbit low spatial frequency error compensation,” *Acta Photonica Sinica*, vol. 49, no. 1, pp. 119–128, Jan. 2020.
[7] M. D. Shuster, “A simple Kalman filter and smoother for spacecraft attitude,” *Astronautical Sci.*, vol. 37, pp. 89–106, Jan. 1989.

[8] M. Samaan, T. Griffith, and P. Singla, "Autonomous on-orbit calibration of star trackers," in *Proc. Core Technol. Space Syst. Conf. (Commun. Navigation Session)*, 2001, pp. 27–30.
[9] H. B. Liu, W. X. Wang, and S. Y. Chen, "Star tracker ground calibration based on the invariant of interstar angles," *J. Nat. Univ. Defense Technol.*, vol. 36, no. 6, pp. 48–52, Dec. 2014.
[10] Z. Wang, J. Jiang, and G. J. Zhang, "Observation angular distance error modeling and matching threshold optimization for terrestrial star tracker," *Opt. Exp.*, vol. 27, no. 23, pp. 33518–33536, Nov. 2019.
[11] J. Enright, I. Jovanovic, and B. Vaz, "On-orbit star tracker recalibration: A case study," in *Proc. IEEE Aerosp. Conf.*, Mar. 2015, pp. 1–13.
[12] J. Enright, I. Jovanovic, and B. Vaz, "Autonomous recalibration of star trackers," *IEEE Sensors J.*, vol. 18, pp. 7708–7720, Jul. 2018.
[13] X. H. Zhen, Z. Z. Wei, and G. J. Zhang, "Angular distance constraints calibration for outdoor zoom camera," *Opt. Exp.*, vol. 24, no. 21, pp. 23898–23910, Oct. 2016.
[14] J. Li, K. Xiong, and X. G. Wei, "A star tracker on-orbit calibration method based on vector pattern match," *Rev. Scientific Instruments*, vol. 88, Apr. 2017, Art. no. 043101.
[15] H. J. Zhong, M. F. Yang, and X. Lu, "Calibration method of star sensor," *Acta Optica Sinica*, vol. 30, pp. 1343–1348, May. 2010.
[16] J. H. Yang, and S. H. Pei, "A high precision camera calibration method for principal point," China Patent CN105258710A, Jan. 2016.
[17] P. W. Nie, and E. H. Liu, "Weighted on-orbit calibration method of principal point and focal length for star sensor," *Appl. Opt.*, vol. 39, no. 6, pp. 827–831, Nov. 2018.
[18] Z. Y. Zhang, "A flexible new technique for camera calibration," *IEEE Trans. Pattern Anal. Mach. Intell.*, vol. 22, no. 11, pp. 1330–1334, Dec. 2000.
[19] R. Y. Tsai, "A versatile camera calibration technique for high accuracy 3D machine vision methodology off-the-shelf camera," *Robot. Automat.*, vol. 3, pp. 323–344, Aug. 1987.
[20] G. Welch, and G. Bishop, An introduction to the Kalman filter. 2001. [Online]. Available: https://courses.cs.washington.edu/courses/cse571/03wi/notes/ welch-bishop-tutorial.pdf
[21] W. Fan, and Y. Li, "Analysis on observable degree of autonomous spacecraft orbit navigation based on SVD method," *Aerosp. Control*, vol. 27, pp. 50–55, Apr. 2009.
[22] L. Wu, and Q. Xu, "A star sensor on-orbit calibration method based on singular value decomposition," *Sensors*, vol. 19, no. 15, p. 3301, Jul. 2019.
[23] C. C. Liebe, "Accuracy performance of star trackers-a tutorial," *IEEE Trans. Aerosp. Electron. Syst.*, vol. 38, no. 2, pp. 587–599, Jan. 2002.